CHEMISTRY
A EUROPEAN JOURNAL

DOI: 10.1002/chem.200500860

# Surface-Functionalized Latex Particles as Controlling Agents for the Mineralization of Zinc Oxide in Aqueous Medium

**Rafael Muñoz-Espí,[a] Yun Qi,[a] Ingo Lieberwirth,[a] Clara M. Gómez,[b] and Gerhard Wegner*[a]**

**Abstract:** Polystyrene latex particles modified at the surface with different hydrophilic functional groups were prepared by miniemulsion polymerization and used as controlling agents in the crystallization of zinc oxide from aqueous medium. The effects of the chemical nature of the surface functionalization and the latex concentration on the crystal growth, morphology, and crystalline structure of the resulting zinc oxide were analyzed. Micro- and submicrosized crystals with a broad variety of morphologies depending on the functionalization were obtained. Among the different latexes studied, the acrylic-acid-derived particles were shown to be a convenient system for further quantitative investigations. In this case, as the additive concentration increases, the length-to-width ratio (aspect ratio) of the crystals decreases systematically. Preferential adsorption of the latex particles onto the fast-growing faces {001} of ZnO is assumed to follow a Langmuir-type isotherm, and interaction of the adsorbed particles with the growth centers will reduce the growth rate in [001]. This leads to a quantitative relationship linking the aspect ratio to the latex concentration at constant diameter and surface chemistry of the latex. The dependence of the aspect ratio on charge density of the latex can also be modeled by an algorithm in which attractive forces between the latex particle and the ZnO surface are balanced against repulsive forces of an osmotic nature. The latter are associated with the confined volume between the crystal and latex particle surfaces.

**Keywords:** crystal growth · latex · morphogenesis · polymers · zinc oxide

## Introduction

Commonly in nature, crystal growth of inorganic systems is controlled by the presence of biogenic macromolecules. Calcium carbonate, present in corals and shells of sea creatures, or calcium phosphates, present in bones or teeth, are typical examples of this phenomenon. Many research groups focus on the investigation of such processes, working in the area of biomineralization.[1–3] However, the study of mineralization phenomena and the growth mechanisms involved is not only interesting for the life sciences, but it has also industrial importance. The control of the crystal growth features of inorganic materials has become an active research field in the last two decades, because of the increasing interest in obtaining materials with homogeneity and specificity of both the crystal shape and the size distributions, key aspects in many applications.[4,5]

This scientific interest has focussed on a limited number of systems, among which the most important are carbonates[6–8] (calcium and barium carbonate), phosphates[9,10] (calcium and zinc phosphates), sulfates[11] (barium sulfate), sulfides[12–16] (zinc and cadmium sulfide), chromates,[17] and several metal oxides[18–20] (aluminum, zinc, titanium, zirconium, and iron oxides). From the mechanistic point of view, zinc oxide is quite an ideal system for studies of the controlled crystallization. Due to its high insolubility in water, ZnO can be easily precipitated from an aqueous solution, and only one modification is obtained (zincite). In addition, this is a versatile material and micro- and nanostructures of zinc oxide are interesting for various applications, such as catalysts, cosmetics, pigments, varistors, electro- and photoluminescence devices, and gas sensors.[21–23] Much research has been devoted to the precipitation of ZnO from aqueous media, investigating the changes in morphologies and prop-

[a] R. Muñoz-Espí, Dr. Y. Qi, Dr. I. Lieberwirth, Prof. Dr. G. Wegner
Max-Planck-Institut für Polymerforschung
Ackermannweg 10, 55128 Mainz (Germany)
Fax: (+49) 6131–379–100
E-mail: wegner@mpip-mainz.mpg.de

[b] Prof. Dr. C. M. Gómez
Institut de Ciència dels Materials
Departament de Química Física, Universitat de València
Dr. Moliner 50, 46100 Burjassot, València (Spain)

erties, and trying to understand the controlling parameters. The effect of the synthetic pathway,[24–27] the reaction parameters (temperature, pH, reaction time, concentration),[28,29] and the influence of different solvents[30,31] have been broadly screened. The use of different organic additives to control the morphology of the resulting crystals has been also reported.[32,33]

As indicated above, biopolymers control the growth of inorganic structures in various life forms. Imitating nature, synthetic polymers have been used as additives in the crystallization of zinc oxide. The presence of double hydrophilic block- and graft-copolymers has been shown to affect the morphology of ZnO crystals obtained from aqueous media.[34–36] Actually, these types of polymers have not only been used in the control of ZnO crystallization, but also extensively applied to other systems, for instance $CaCO_3$ or $BaSO_4$. A systematic overview of the different systems in which the crystallization has been controlled by hydrophilic polymers can be found in a recent review published by Yu and Cölfen.[37]

The effects observed with hydrophilic polymers prompt the investigation of a system with functional groups anchored to the surface of spherical latex particles. Latex particles, prepared by miniemulsion polymerization, provide an interesting approach to control crystal growth, as indicated by preliminary results.[36] These particles are versatile, as the particle size and the local concentration of functional groups attached to the surface can be controlled. Furthermore, the synthesis of latex particles is convenient, reproducible, and structures with surfaces of various chemical compositions can be obtained quickly from simple monomers.

Here, we focus on the influence that the structure and the content of latex additives have on the crystal growth of zinc oxide precipitated from an aqueous solution, and explore the nature of the control parameters.

## Results and Discussion

**Synthesis and characterization of surface-functionalized latexes**: Following the basic procedure of Landfester et al.,[38,39] latex particles typically of radii 30–120 nm were prepared by direct miniemulsion polymerization, using ultrasonication as a shear method to achieve the state of miniemulsion. Styrene, practically immiscible in water, was the main component of the oil phase, and the various comonomers **1** to **6** were used to modify the surface properties of the latex particles, considering the polarity and the charges of their functional groups.

A non-ionic poly(ethylene oxide)-derived surfactant, Lutensol AT50, $(C_{16}H_{33})(EO)_{50}$,[40] was used instead of cationic or anionic surfactants, to minimize any undesired effect in the ZnO crystallization. Hexadecane was used as a hydrophobic agent to stabilize the emulsion and to avoid Ostwald ripening. This costabilizer has been reported to disperse homogeneously in the droplets and it does not show any enrichment close to the interface.[41]


acrylic acid (**1**) maleic acid (**2**) ethylene glycol methacrylate phosphate (**3**)

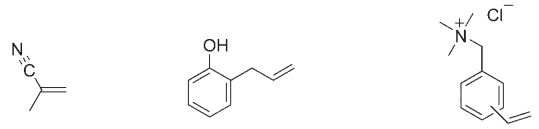


methacrylonitrile (**4**) 2-allylphenol (**5**) vinylbenzyl trimethylammonium chloride (**6**)

To commence the polymerization inside the droplets, an oil-soluble initiator, 2,2′-azobis(2-methylbutyronitrile) (AMBN), was used. AMBN was preferred to the typical AIBN (2,2′-azoisobutyronitrile) because of its higher insolubility in water. In some cases (explicitly indicated), small portions of the water-soluble initiator potassium persulfate ($K_2S_2O_8$) were added to initiate the polymerization of water-soluble comonomers in the aqueous phase and to improve their grafting onto the corona.

The miniemulsification leads to the formation of small droplets of the oil phase (containing mainly styrene, hexadecane, and the initiator), partially covered by the surfactant, which stabilizes the miniemulsion. The hydrophilic comonomer is outside the droplets in the aqueous phase, but due to its partition coefficient, a small fraction is also present in the oil phase. Because of this, copolymerization of the hydrophilic monomer with the styrene may also take place inside the droplets. As an example, let us consider acrylic acid (AA) as the hydrophilic monomer for the following discussions. There is always an equilibrium between the AA present outside and inside the droplets, and as AA units polymerize in the oil phase, new molecules diffuse from the aqueous to the oil phase. As soon as AA becomes incorporated into the growing chain, mainly composed of styrene units, the chain assumes an amphiphilic character and moves toward the interface to expose the carboxyl groups to the water phase. As a consequence, a complex latex corona structure is formed. As sketched in Figure 1, the latex corona is comprised of short segments of the hydrophilic component of the non-ionic surfactant and hydrophilic segments of the copolymer between styrene and AA. A certain concentration of carboxylic groups will be present embedded at various depths inside the corona. The details of the structure and properties of the corona in core-shell latexes, formed as a consequence of analogous or similar processes, are still not fully understood and have been the subject of detailed studies (e.g., references [42–47]). In our case, we are mainly concerned with the density of functional groups that can be accommodated by a growing crystal surface, assuming that these functional groups need to make contact with the surface in order to control the crystal-growth features.

  

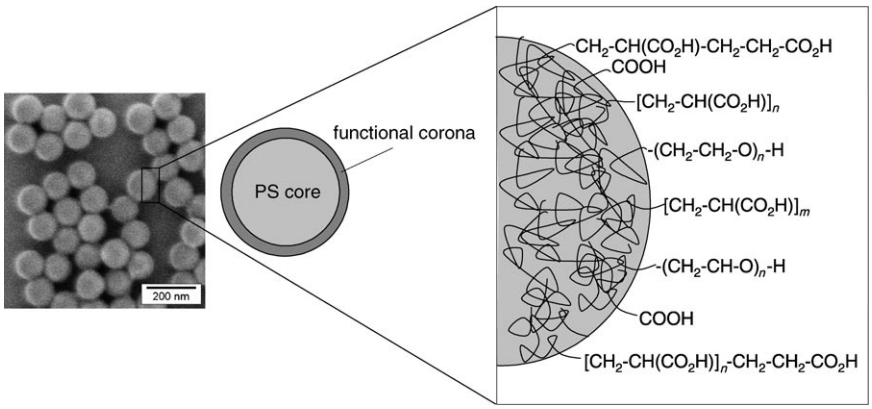


Figure 1. SEM micrograph of a poly(styrene-acrylic acid) latex and schematic representation of the chemistry of the corona.

In this work, it is assumed that copolymerization processes similar to the one described for the case of AA occur for the other comonomers used. In the case of methacrylonitrile and 2-allylphenol, with solubilities in water of only 25.7 and 7 g $L^{-1}$, respectively (at 20 °C), it is expected that the segments composed of these monomers will generally remain inside the latex core, and only a small fraction will be present within the corona.

Surface-charge densities of the latex particles were determined by performing direct polyelectrolyte titration (also called colloid titration), based on the interaction between oppositely charged polyelectrolytes.[48,49] Poly(diallyl dimethylammonium chloride) (poly-DADMAC) was used as titrating agent and the carboxylic groups were previously deprotonated by adjusting the pH to values of approximately 9.5. The final point of the titration was detected by using a particle-charge detector (PCD), whose operating system is based on electrokinetic measurements.[50] It has been reported that, in this technique, the type of functional groups plays an important role, and the measured density of charges may differ from the real value.[49] Nevertheless, this method gives insight into the differences between latex preparations, and the charge-density estimation provided is sufficient for our requirements. The diameters (from photon correlation spectroscopy measurements[51]) and results of polyelectrolyte titrations for latex emulsions prepared with the different hydrophilic comonomers (samples **S1** to **S6**), as well as the diameter of a non-charged reference latex (sample **S0**), are compiled in Table 1. This table also shows those cases in which potassium persulfate was used in a second step of the reaction. The reaction parameters for all the samples reported in the table were chosen so that particle diameters in the range of 60–90 nm and surface-charge densities of approximately 0.5–2.0 $nm^{-2}$ were obtained.

Table 1. Characteristic data of latex samples obtained by miniemulsion copolymerization of styrene (**S**) with various comonomers (**1**–**6**).[a]

| Sample | Functional comonomer | Initiator | Diameter [nm] | Surface-charge density[b] [$nm^{-2}$] |
|---|---|---|---|---|
| **S0** | – | AMBN | 59 | 0.0 |
| **S1** | **1** | AMBN | 72 | 1.4 |
| **S2** | **2** | AMBN/$K_2S_2O_8$ | 79 | 0.6 |
| **S3** | **3** | AMBN/$K_2S_2O_8$ | 80 | 2.3 |
| **S4** | **4** | AMBN | 73 | n.d.[c] |
| **S5** | **5** | AMBN | 91 | n.d.[c] |
| **S6** | **6** | AMBN/$K_2S_2O_8$ | 80 | n.d.[c] |

[a] The reaction mixture contained 96 wt% of styrene and 4 wt% of each comonomer, except for **S0**, in which only styrene was used. The solid content was 22 ± 1 wt% after polymerization, except in the case of sample **S5**, in which the solid content was 11 wt%. [b] Determined by polyelectrolyte titration and expressed as charged groups per unit area. [c] n.d. = not determined.

**Screening of different surface-functionalized latexes for morphology control**: Zinc oxide crystallizes in the hexagonal system as zincite ($a = 3.2498$ Å, $c = 5.2066$ Å, space group $P6_3mc$, number of formula unit $Z = 2$, $\rho = 5.68$ g $cm^{-3}$). The oxygen atoms are hexagonal close-packed, and the zinc atoms occupy half of the tetrahedral interstices and are also hexagonal close-packed. This mode of crystal packing is shown in Figure 2a.

The crystal structure readily implies that the faces normal to the *c*-axis, (001) and (00$\bar{1}$), exhibit a highly polar character and are not identical under ideal conditions. The (001) face is composed of zinc atoms, whereas the (00$\bar{1}$) face is occupied by oxygen atoms. Under conditions of growth from an aqueous medium these surfaces may be hydrated,[52] but will still differ with regard to polarity and charge density. In fact, we observe the formation of twins in almost all cases, which may be a consequence of the instability of one of these polar faces. A structure of this twin formation is sketched in Figure 2b. The ZnO structure contains also a series of non-polar faces {*hk*0}, electronically neutral, with equal numbers of oxygen and zinc atoms.

In this work, zinc oxide was precipitated from an aqueous solution of zinc nitrate by adjusting the pH through the thermal decomposition of hexamethylenetetramine (HMTA) in ammonia and formaldehyde at the reaction temperature of 95 °C. Before the start of the precipitation reaction, the pH has a value of around 5 in the absence of additives. This initial pH can change considerably as the functionalized latexes are added. However, independent of the initial value, HMTA produces a buffer effect and the final pH remains constant at around 6.

In a conventional precipitation in the absence of any additive, long hexagonal prismatic crystals are formed. This morphology, reproduced in Figure 3a, implies that different crystal faces grow with different velocities. It can be deduced that the basal face (001) is a rapidly growing face and

  

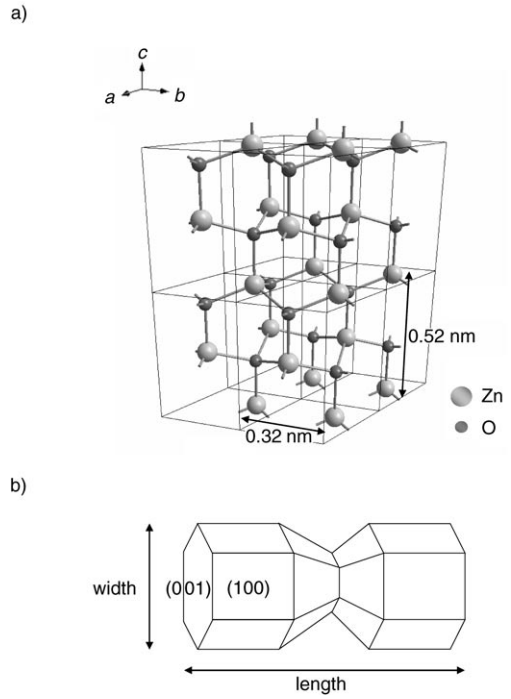


Figure 2. a) Structure of ZnO (zincite). b) Crystal habit frequently observed in controlled precipitation, with definition of experimental magnitudes (length and width) and crystal faces (basal face (001) and lateral face (100)).

the lateral faces {*hk*0} are slow growing, which results in a needlelike crystal.

Polyelectrolytes may adsorb onto the surface of growing crystals and modify the growth features. In this context, surface-functionalized latexes represent an interesting approach, as indicated in the Introduction. For this reason, we initially screened the effect of latex particles differently functionalized at their surface, but with similar particle dimensions.

The precipitations were carried out in a medium containing $1\,g\,L^{-1}$ of latex (content of solid latex in the total volume), which represents a particle density of approximately $2\times10^{13}$ per $cm^3$ (considering an average radius of 35 nm and approximating the density of the solid latex to $1\,g\,cm^{-3}$). In general, the latex particles are embedded in the growing crystal, becoming incorporated into the structure and giving ZnO–latex hybrid materials. If desired, the latex can be removed by dissolving with organic solvents or, more effectively, by calcination.

The resulting morphology of the crystals was investigated by conducting scanning electron microscopy (SEM). Figure 3 shows how the SEM micrographs of the various experiments compare with the reference sample.

A brief description of the main observations of the screening experiments follows:

a) The reference sample in Figure 3a shows a high probability of occurrence of starlike growth features that are the result of nucleation of several individual crystals from the same nucleation center. Small, needlelike crystals resulting from secondary nucleation processes are observed.

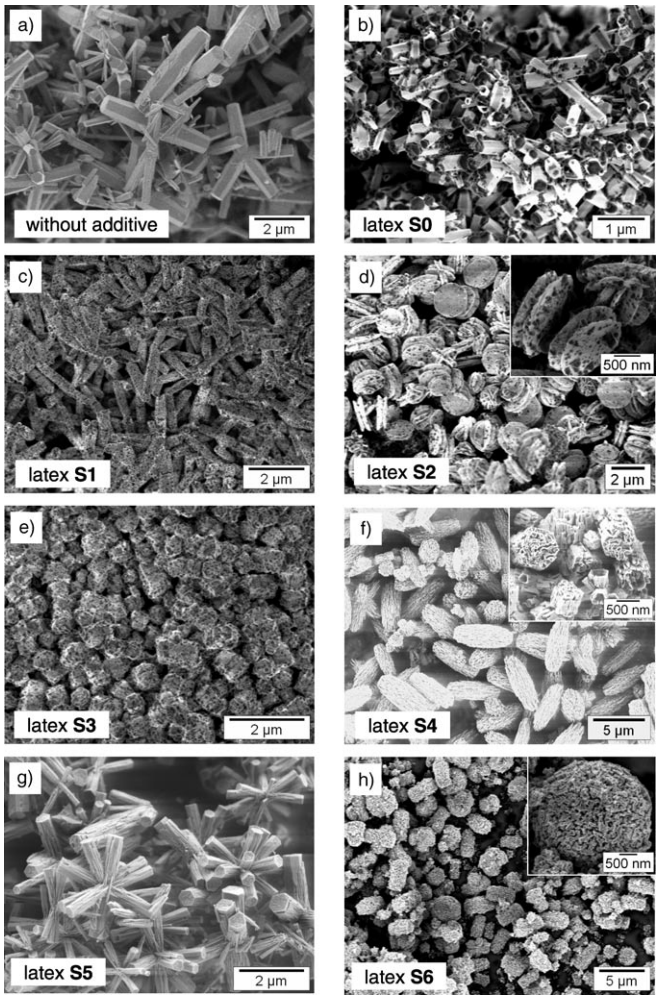


Figure 3. Zinc oxide samples crystallized (a) without additive, and (b–h) in the presence of $1\,g\,L^{-1}$ of the latexes **S0** to **S6**, respectively (see Table 1). The samples shown in (f) and (h) were calcinated at 600 °C to remove the polymer.

b) Upon addition of a pure polystyrene latex (latex **S0**), without addition of functional groups to its surface, the crystals show essentially the same morphology as the reference sample, composed of hexagonal prismatic crystals of widely differing length-to-cross-section ratio. A few of the latex particles remain adsorbed on the surface.

c) With poly(styrene-acrylic acid) latex (latex **S1**), crystals with lower polydispersity in the dimensions are obtained. The crystals are densely covered by latex particles that could not be removed by simple washing, as was the case for the latex **S0**. This indicates a strong interaction between the surface groups of the latex particles and the zinc oxide.

d) The addition of poly(styrene-maleic acid) latex (latex **S2**), with two carboxylic groups in the functional monomer, leads to crystals with a completely different mor-

  

phology. The crystals show a platelike shape and no clear borders are formed; the hexagonal structure essentially disappears. However, the twinning and the starlike growth of the crystals from a common nucleation center are present, as in previous samples. A relatively high number of latex particles remain in the crystals after washing.

e) With poly[styrene-(ethylene glycol methacrylate phosphate)] latex (latex **S3**), the obtained prismatic crystals were shorter and wider, with a more isometric morphology, that is, with similar length and width. The interaction of the latex particles with ZnO appears to be strong, as in the case of the latex **S1**, and the crystals are densely covered with the polymeric nanoparticles.
f) Very large amounts of aggregated poly(styrene-methacrylonitrile) latex (latex **S4**) were observed upon using this additive, and the analysis of the crystal structure was only possible after calcinating the polymer. Figure 3 f shows peculiar "canal structures" observed in the resulting crystals after pyrolysis at 600 °C (10 °C $min^{-1}$, from room temperature to 600 °C).
g) In the presence of the poly[styrene-(2-allylphenol)] latex (latex **S5**), starlike hexagonal crystals are again obtained, and no residual polymer is observed. This indicates that the latex does not adsorb onto the crystals and it is completely removed during the centrifugation and washing processes.
h) As in the case of the latex **S4**, analysis of the morphology of the crystals precipitated in the presence of the positively charged latex based on vinylbenzyl trimethylammonium chloride (latex **S6**) was only possible after removal of the latex by pyrolysis. Very porous crystals with "canal structures" are observed after calcination.

In spite of the very different external morphologies, all our products were analyzed by X-ray diffractometry (XRD) and clearly identified as pure zincite (JCPDS 36–1451), without contamination by other crystalline species.

**Influence of the latex concentration on the crystal morphology**: The latex concentration appears to be an important parameter for the final morphology of the ZnO crystals, as is shown in Figure 4. By using acrylic-acid-functionalized latex **S1** as the crystallization additive, the length-to-width ratio decreases systematically as the concentration increases.

The latex **S2**, synthesized from maleic acid, produced a very strong effect in the crystals obtained. The significant differences in the morphologies for the latexes **S1** and **S2** cannot be justified only in terms of the number of carboxylic groups, because the effect is much higher than that expected for such surface-charge densities. In the presence of an increasing concentration of the latex **S2**, the growth in the *c*-axis is blocked and the crystals become wider until thin laminar structures are observed. If one naively assumes that the latex is reversibly adsorbed onto the (001) plane and that the rate of growth in the *c*-direction is proportional to the actual coverage by the latex particles (this is discussed in detail below), then the absorption constant for the maleic-acid-functionalized latex must be much higher than that for the latex exposing acrylic acid groups towards the growth plane. In the latter case, prismatic crystals are obtained, and suppression of the growth of this plane leads to platelike crystals. The strong affinity in the case of the maleic-acid-derived latex may be explained by taking into account the special conformation that the polymeric chains can take due to the *cis* position of the two carboxylic groups in the monomer. This conformation will not occur in the latex based on

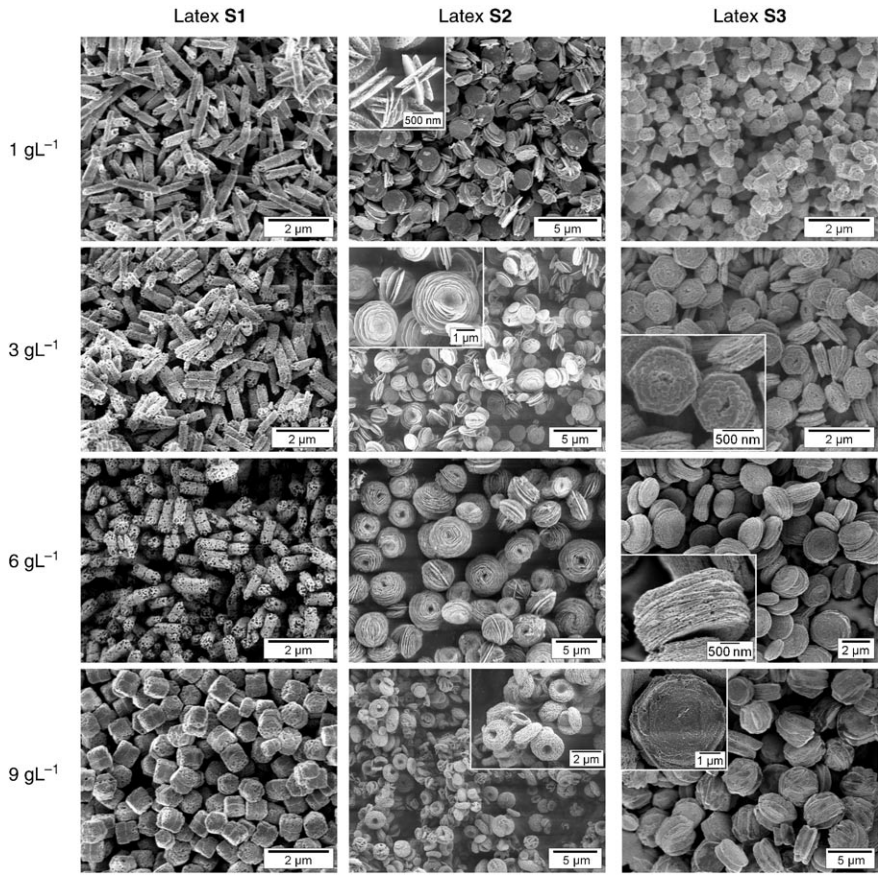


Figure 4. SEM micrographs of samples crystallized at different concentrations of the latexes **S1**, **S2**, and **S3** (see Table 1). The latex was eliminated by calcination at 600 °C.

  

acrylic acid, in which very high concentrations of the latex (ca. 9 $gL^{-1}$) are required to substantively reduce the aspect ratio.

The phosphate groups attached to the surface in the latex **S3** have an intermediate effect, not as strong as in the case of the maleic-acid-derived functionalities, but stronger than in the acrylic-acid-type residues. Comparing the effects of the acrylic acid and the phosphate-group-decorated latexes, one sees that a concentration of 1 $gL^{-1}$ in the first case produces approximately the same effect as a concentration of 9 $gL^{-1}$ in the latter. At a concentration of 6 $gL^{-1}$, laminar structures can be observed, similar to those obtained in the presence of the latex **S2**.

**Poly(styrene-acrylic acid) latex as crystallization additive**

From the results of the screening described above, the poly(styrene-acrylic acid) (PSAA) latex appears to be a convenient system for a more detailed study, for the following reasons: i) the particles are incorporated into the crystals without formation of large polymer aggregates; ii) the prismatic form of the resulting crystals allows the measurement of width and length, facilitating the quantification of the effect of the additive; iii) good estimation of the surface-charge density of the latex can be obtained by titration with poly-DADMAC, which may become more difficult for latex with other functional residues, for instance phosphate groups. Therefore, to analyze the influence of the latex concentration on the morphology and the crystal habit, samples in the presence of different quantities of PSAA latex were crystallized.

*Morphology and crystalline structure*: The aspect ratio ($A$), defined as the quotient of the length and the width, undergoes a systematical decrease as the PSAA latex concentration increases, as shown in Figure 4. The width and length of the crystals in each sample were determined from statistical analysis of SEM images, after measuring at least 100 particles. Histograms of the length and width distributions were obtained for each sample; these are plotted in Figure 5. The presence of the latex reduces the length distribution from multimodal to monomodal, even at the smallest concentration of 0.5 $gL^{-1}$. Further increase of the latex concentration reduces the length of the crystals taken at the maximum of the length distribution curve, which was used to describe the envelope of the histograms. Note that a single normal distribution is sufficient to describe the statistical data and that the width of the distribution becomes narrower as the latex concentration increases. The width distribution is rather narrow to begin with, but the mean value increases systematically as the latex concentration increases. In other words, the crystals become more isometric. The aspect ratio $A$ was calculated from the average length-to-width ratio of the data shown in Figure 5, and it is plotted in Figure 6. The product of the square of the width and length of the crystals remains approximately constant within the limits of error, indicating that the volume of the growing crystals in the system is not significantly affected by the change in latex concentration. Considering that all data were obtained from comparable reaction yields, this implies that the number of crystals in the system remains the same for different latex concentrations.

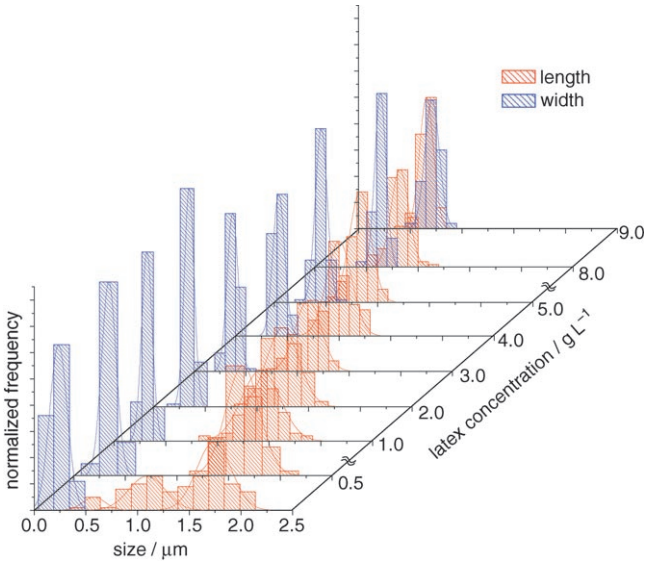


Figure 5. Histograms of the lengths and widths of crystals in samples grown in the presence of different concentrations of the PSAA latex **S1**.

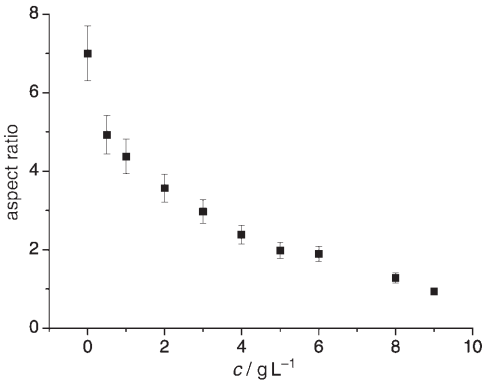


Figure 6. Relationship of the aspect ratio to the concentration of PSAA latex **S1**.

Changes in the crystal morphology do not imply significant changes in the microcrystalline structure, as can be deduced from the XRD data shown in Figure 7. Here, powder diffractograms of samples whose morphologies were analyzed to obtain the data of Figures 5 and 6 are presented. Assuming that the peak broadening results only from the size of the coherently scattering domains, their size can be estimated by using the Scherrer equation [Eq. (1)],[53]

$$L_{hkl} = \frac{K\lambda}{\beta_{1/2}\cos\theta} \quad (1)$$

  

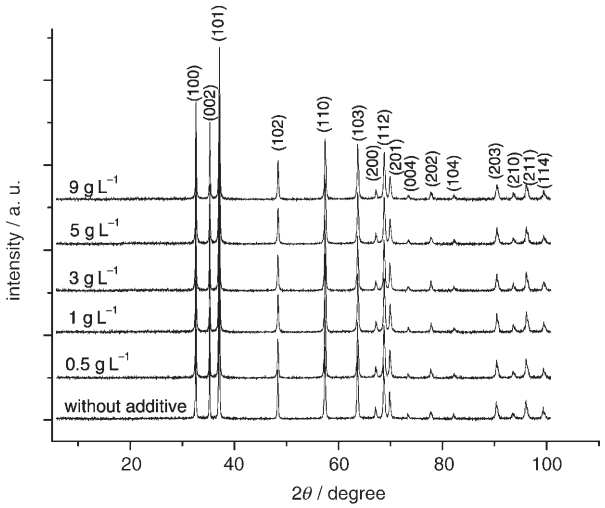


Figure 7. X-ray diffractograms of ZnO crystallized in the presence of different concentrations of the PSAA latex **S1**, as indicated; the samples contained up to approximately 10 wt% of latex occluded in the crystals (see Table 2).

in which $K$ is a form factor approximately equal to unity, $\lambda$ is the radiation wavelength (1.54 Å), and $\beta_{1/2}$ is the full width at half maximum (FWHM) of the peak on the $2\theta$ scale in radians. This equation was applied to the (100) and (002) reflections, after normalizing and adjusting to Lorentzian (Cauchy) curves,[54] which may be taken as an approximation to fit XRD reflections.[53] The positions of these two reflections and the FWHM are listed in Table 2, together with the estimated crystallite sizes. The latex content in the final products, that is, the quantity of latex incorporated from the initial latex concentrations added during the crystallization, is also listed. The amount of latex occluded in the crystals was estimated from the weight loss determined by thermogravimetrical analysis (TGA).

Table 2. Position and full width at half maximum ($\beta_{1/2}$) of the (100) and (002) reflections in ZnO crystals obtained in the presence of different amounts of the latex **S1** (see Table 1). Crystallite sizes ($L_{hkl}$) were calculated by using the Scherrer equation [Eq. (1)], and the latex content was estimated from the weight loss determined by TGA.

| Sample | Latex | Latex content | (100) | | | (002) | | |
|---|---|---|---|---|---|---|---|---|
| | [g L$^{-1}$] | [%] | $2\theta$ [°] | $\beta_{1/2}$ [°] | $L_{100}$ [nm] | $2\theta$ [°] | $\beta_{1/2}$ [°] | $L_{002}$ [nm] |
| ZL0 | 0 | 0 | 31.750 | 0.111 | 83 | 34.408 | 0.097 | 95 |
| ZL05 | 0.5 | 1.7 | 31.764 | 0.156 | 59 | 34.420 | 0.136 | 68 |
| ZL10 | 1.0 | 4.3 | 31.785 | 0.163 | 56 | 34.436 | 0.130 | 71 |
| ZL30 | 3.0 | 7.0 | 31.765 | 0.174 | 53 | 34.411 | 0.127 | 73 |
| ZL50 | 5.0 | 9.1 | 31.804 | 0.177 | 52 | 34.459 | 0.147 | 63 |
| ZL90 | 9.0 | 9.5 | 31.811 | 0.145 | 63 | 34.464 | 0.139 | 66 |

As the latex concentration increases, the $2\theta$ values tend to shift to slightly smaller angles (considering the maximum of the Lorentzian fittings) and the peaks tend to broaden. Crystallite sizes calculated by using the Scherrer equation [Eq. (1)] decrease as the additive concentration increases. However, it should be mentioned that the shifts in the position are small and close to the resolution limit of the X-ray diffractometer used. In general, it can be concluded that the long-range order in the crystals is not disturbed. Thus, the use of latex as additive causes no significant reduction in the perfection of the crystals.

*Model considerations*: The change in morphology that accompanies increasing latex concentration can be explained by a model of the interaction between the latex particles and the growing faces of the zinc oxide. Presumably, the latex particles, functionalized on the surface with carboxylic groups, are adsorbed preferentially onto the (001) face of zincite, thereby blocking the positions from which the crystal would normally tend to grow. This leads to a slower growth along [001], although other possible growth directions are essentially not affected. If it is assumed that the latex particles adsorb onto the basal plane (001) according to a Langmuir isotherm (i.e., a surface coverage proportional to the overall concentration is achieved), then the fraction of the surface covered by latex (normalized to 1), $\theta$, is given by Equation (2),

$$\theta = \frac{kc}{1+kc} \tag{2}$$

in which $k$ is the adsorption constant and $c$ is the concentration of latex particles. Above a certain concentration, full coverage of the basal plane by the latex spheres will be achieved. This will define the maximum of the effect. At lower concentrations, the crystals will grow along [001] in proportion to the fraction of free surface available for the addition of crystal-building species. We assume that the aspect ratio is proportional to the free surface available at a certain coverage defined by $\theta$. This requires a rescaled aspect ratio, $S$, defined by Equation (3),

$$S = 1 - \frac{A_c - A_\infty}{A_0 - A_\infty} \tag{3}$$

in which $A_c$ is the aspect ratio at a certain latex concentration, $A_\infty$ is the aspect ratio at an infinitely large latex concentration, and $A_0$ is the aspect ratio obtained in the absence of latex. The rescaled aspect ratio $S$ for the data of Figure 5 is plotted in Figure 8, by adjusting the data to a function equivalent to the Langumir isotherm [Eq. (4)].

$$S = \frac{k'c}{1+k'c} \tag{4}$$

It can be observed that the model correlates quite well with the data for latex concentrations of below 6 g L$^{-1}$, but for higher concentrations, the experimental values differ from the theoretical curve. At high concentration, more

  

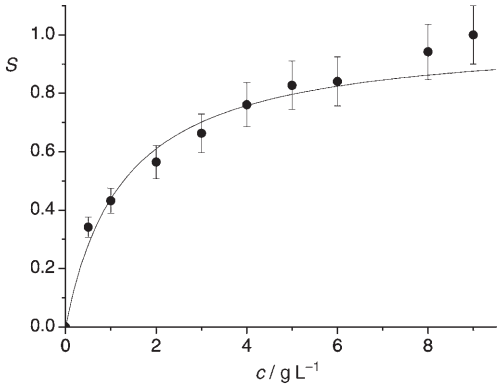


Figure 8. Plot of the scaled aspect ratio $S$ (see [Eq. (3)]) versus the concentration of latex, $c$, following the algorithm of a Langmuir isotherm (see [Eq. (4)]).

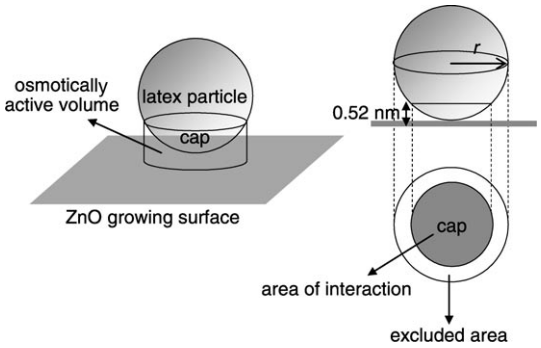


Figure 9. Schematic representation of the "cap model" for adsorption of a latex particle at the ZnO surface.

complex phenomena, such as multilayer adsorption, may occur, complicating the treatment. By excluding the points for $c > 6\,g\,L^{-1}$, the value obtained for the constant $k'$ was $0.78 \pm 0.05$. Because the adsorption of the latex is related to the surface-charge density, different values of $k'$ would indicate different characteristics of the latex particles.

The aspect ratio of the resulting crystals is influenced mainly by two parameters: the concentration and the surface-charge density of the latex particles. So far, we have considered a fixed surface charge of the latex particles and a variable additive concentration. Another series of experiments was carried out in which the surface-charge density was altered to investigate quantitatively the influence of this parameter. From here on, the latex particles are considered as spheres of radius $r$ with an average surface charge. It is assumed that no deformation of the spherical shape occurs during the adsorption process. The characteristic length scale for features relative to defects that control the growth of crystals is the Burgers vector, that is, the height $h$ of the growth spirals is responsible for growth in a particular direction. Carboxylic groups at a distance greater than $h$ will not be able to interact with the growth sites on the ZnO surface. In this context, we can define a "cap" of the latex sphere as being the region where the functional groups interact with the crystal surface. The meaning of the cap is further demonstrated in Figure 9. The surface area of this "cap" is denoted as $2\pi rh$. As an approximation, the value of the height $h$ is set as 0.52 nm, which corresponds to the unit-cell parameter $c$ of zincite; other values would result in only a proportional rescaling. The number of carboxylic groups per "cap", $N$, can be calculated by multiplying the surface-charge density by the surface area of the "cap". This value $N$ allows us to eliminate the effect of the diameter of the latexes as an independent parameter.

By taking the Langmuir-type dependence of the aspect ratio into account, two different situations were considered:

1) a small concentration of latex of $0.6\,g\,L^{-1}$, meaning a linear dependence of $A$ on $c$ (i.e., $k'c \ll 1$)
2) a higher latex concentration of $6\,g\,L^{-1}$, that is, close to the saturation value ($k'c \cong 1$).

The same type of PSAA latex as in the previous experiments was used; however, the parameters of the synthesis were tuned to obtain samples that differed in both surface-charge density and diameter. The set of prepared latexes is listed in Table 3, together with the resulting aspect ratios of the ZnO crystals obtained at the two different latex concentrations of 0.6 and $6\,g\,L^{-1}$. As described previously, the aspect ratio was calculated from the statistical treatment of SEM micrographs. The aspect ratios obtained are plotted in Figure 10 as a function of $N$. The solid lines through the points were calculated on the basis of the considerations presented below. Both curves show a similar behavior: in region I, the aspect ratio decreases dramatically as $N$ increases towards a minimum located at ~100 charged groups per cap; in region II, the aspect ratio increases again until it reaches a constant value that is maintained in region III. Note that the minimum aspect ratio occurs at a similar value of $N$ for both sets of experiments, that is, the minimum seems to be independent of the latex concentration; in other words, only the associated value of the aspect ratio reflects the concentration.

As indicated above, the two parameters influencing the aspect ratio are the latex concentration and the number of charged groups per "cap" ($N$). In reality, Figures 5 and 10 are actually sections through a multiparameter space.

The experimental points of Figure 10 are approximated by a curve calculated according to the following considerations. It is assumed that the interactions occurring within a certain volume between the latex and the ZnO surface control the adsorption process. This volume is referred to as the "osmotically active volume" and is defined as the projection of the "cap" onto the ZnO growth plane. The variable is the distance between the center of the latex sphere and the ZnO surface. As the sphere approaches the ZnO surface, both attractive and repulsive forces are encountered. At fixed size and surface-charge density, the number of bonds that eventually lead to chemisorption (or physisorption) of the sphere onto the surface is, therefore, well defined. One could assume, for the sake of simplicity, that ionic bonds are

  

Table 3. Set of PSAA latexes prepared with different particle diameters and different surface-charge densities, together with the average aspect ratio of the zinc oxide crystals obtained at latex concentrations of 0.6 and 6 g L$^{-1}$. The latexes are listed according to increasing number of charged groups on the "cap".

| Latex sample | Diameter [nm] | Surface-charge density [nm$^{-2}$] | Number of charged groups on "cap" | Aspect ratio at 0.6 g L$^{-1}$ latex | Aspect ratio at 6 g L$^{-1}$ latex |
|---|---|---|---|---|---|
| SAA1 | 113 | 0.1 | 11 | 3.8 | 2.1 |
| SAA2 | 68 | 0.5 | 54 | 4.2 | 0.7 |
| SAA3 | 82 | 0.4 | 55 | 3.7 | 0.7 |
| SAA4 | 96 | 0.4 | 69 | – | 1.7 |
| SAA5 | 66 | 0.8 | 85 | 3.4 | 0.4 |
| SAA6 | 118 | 0.4 | 85 | – | 3.1 |
| SAA7 | 98 | 0.6 | 101 | – | 2.9 |
| SAA8 | 112 | 0.6 | 103 | – | 0.3 |
| SAA9 | 84 | 0.9 | 120 | 3.5 | 0.4 |
| SAA10 | 115 | 0.8 | 150 | – | 0.5 |
| SAA11 | 116 | 0.8 | 153 | – | 0.5 |
| SAA12 | 83 | 1.2 | 163 | 3.5 | – |
| SAA13 | 97 | 1.1 | 171 | 3.7 | 0.6 |
| SAA14 | 167 | 0.7 | 182 | 4.5 | – |
| SAA15 | 160 | 4.5 | 188 | 3.8 | 0.7 |
| SAA16 | 124 | 1.0 | 192 | 4.2 | 0.7 |
| SAA17 | 121 | 1.0 | 192 | – | 2.0 |
| SAA18 | 116 | 1.0 | 192 | – | 1.6 |
| SAA19 | 84 | 1.4 | 193 | 4.0 | – |
| SAA20 | 120 | 1.0 | 194 | 4.2 | – |
| SAA21 | 84 | 1.6 | 215 | 4.2 | – |
| SAA22 | 104 | 1.4 | 229 | 4.1 | – |
| SAA23 | 134 | 1.1 | 230 | 3.9 | – |
| SAA24 | 192 | 0.8 | 249 | 4.1 | 2.9 |
| SAA25 | 125 | 1.3 | 264 | 4.6 | – |
| SAA26 | 104 | 1.6 | 265 | – | 1.9 |
| SAA27 | 93 | 1.8 | 280 | 4.4 | – |
| SAA28 | 130 | 1.9 | 410 | 4.8 | – |
| SAA29 | 162 | 1.7 | 457 | 4.5 | 4.1 |
| SAA30 | 162 | 2.1 | 564 | 5.0 | 3.5 |
| SAA31 | 100 | 3.9 | 642 | 4.9 | – |
| SAA32 | 92 | 4.6 | 694 | 4.7 | – |
| SAA33 | 236 | 2.8 | 1089 | 4.8 | 3.0 |

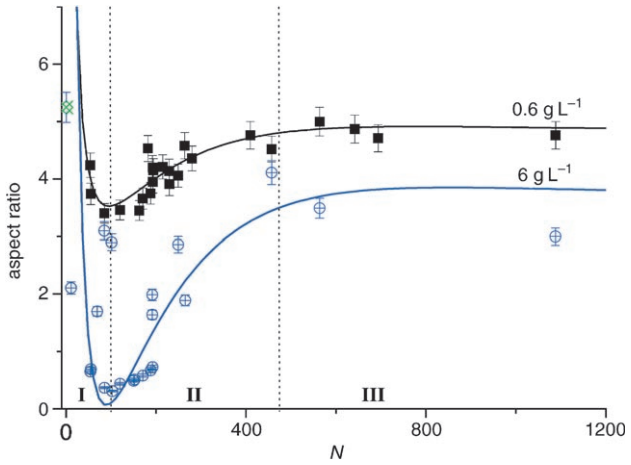


Figure 10. Dependence of the aspect ratio of the ZnO crystals obtained in the presence of PSAA latex particles (at concentrations of 0.6 and 6 g L$^{-1}$) on the number of charged groups on the "cap", $N$.

formed between the carboxylate groups on the surface of the "cap" and the $Zn^{2+}$ species situated within the growth surface. A cut-off length of these interactions is somewhat deliberately defined by fixing the height of the "cap" to 0.52 nm, as already indicated. However, increasing this value would not affect the principal conclusions.

The repulsive forces are dominated by the osmotic pressure that builds up from the confinement of the counterions within the osmotically active volume. These counterions originate from both the carboxylate groups at the surface of the "cap" and the ionogenic groups contained within the ZnO growth surface.

The total interaction potential $V_{total}$ between a sphere and the ZnO growth surface is assumed to be additive, as represented in Equation (5),

$$V_{total} = V_{att} + V_{rep} \quad (5)$$

in which $V_{att}$ and $V_{rep}$ are expressions for the global attractive and repulsive components, respectively, of the total potential. This formulation has some similarities to the DLVO theory, which describes the interaction between colloidal particles.[50,55]

As indicated, the aspect ratio, $A$, is controlled by the adsorption of the latex spheres, with the adsorption constant being a measure of the interaction potential. In Equation (6), we propose the following relationship,

$$A = \frac{a}{N} - \frac{b}{k} e^{-kN} + C \quad (6)$$

in which $k$ and $C$ are constants and $a$ and $b$ are parameters dependent on the latex concentration. The first term of the equation ($a/N$) describes the attractive forces that cause the aspect ratio to decrease as the surface-charge density increases, which is conditional upon small loadings of the surface with carboxylic groups. The second term describes the repulsive forces, related to the osmotic pressure, which increase as the number of carboxyl groups increases. The osmotic pressure could be considered to act as an activation barrier to the adsorption process. The third term is a constant related to the situation of "overloading" of the surface of the spheres with charged groups. The fitting of the experimental points to Equation (6) was performed after estimating the constant $C$ from the average value of the data at $N \geq 500$. The optimization of the fitting parameters gave the

  

following values for latex concentrations of 0.6 and 6 $g L^{-1}$, respectively: 162 and 343 for *a*, 0.032 and 0.073 for *b*, 0.0061 and 0.0059 for *k*, and 4.75 and 3.53 for *C*.

## Conclusions

It is well known that hydrophilic and water-soluble polymers are able to interfere with the nucleation and growth of inorganic crystals during precipitation from an aqueous medium. Double hydrophilic block- or graft-copolymers have been shown to be particularly effective if the functional groups (e.g., carboxylic groups) are spatially separated from other groups (e.g., ethylene oxide groups) that merely facilitate water compatibility without interacting with the surface of the inorganic material. Here, we have demonstrated that for the precipitation of zinc oxide, anchoring of the components of double hydrophilic block- or graft-copolymers to the surface of latex particles has the same effects. Whereas the synthesis of bishydrophilic block- or graft-copolymer may be cumbersome, the application of surface-functionalized latexes offers new possibilities in the control of crystallization phenomena. Latex particles of defined diameter and composition of surface-anchored functional groups are readily and efficiently available by the miniemulsion polymerization technique. The properties of the materials obtained in the course of crystallization of zinc oxide are particularly suited for systematic studies, because zincite is the only polymorph formed and it crystallizes in the form of hexagonal prismatic crystals. The length-to-width ratio of these crystals (aspect ratio) is their most important characteristic feature, and is subject to control by the polymer additive. In addition, latex particles become incorporated into the growing crystals. Thus, hybrid materials can be obtained that are composed of inorganic and largely undisturbed crystalline materials in which organic latex particles are embedded.

The systematic screening of variations in the chemical composition of the corona of the latex particles reveals that both the chemistry of the functional groups and their density are important control parameters that allow the shape of precipitated zincite to be modified from slender elongated to platelike forms. Furthermore, the size distribution of the crystals becomes narrow and homogeneous.

Polystyrene miniemulsion latexes with a corona composed of carboxylic groups (originating from acrylic acid used as comonomer) and oligo(ethylene oxide) residues (from the surfactant used in the preparation of the miniemulsion) have evolved from the screening procedure as a model system.

The diameter of the latex spheres can be easily controlled by choosing the conditions of synthesis. Thus, the diameter of the latex particles and their surface composition in terms of the number of carboxylic groups per unit area are independent parameters subject to variation. Our experiments indicate that the diameter of the latex particles is a "hidden" control parameter, accounted for by considering an interaction volume between the latex particle and the growth surface of the crystals onto which the particle is adsorbed. The number of active groups, *N*, within the area of the "cap" of the spherical latex particles can be defined; functional groups outside the area of the cap have no opportunity to interact with a surface of the crystal.

The aspect ratio of the prismatic zinc oxide crystals is a function of the latex concentration, all other parameters are kept constant. A model that assumes absorption of the latex particles onto the growth centers at the basal plane of zincite according to a Langmuir isotherm can explain the dependence of the aspect ratio on the overall latex concentration.

The influence of other control parameters, that is, the curvature (radius) and density of functional groups at the surface, can be combined and accounted for in the definition of "active groups" *N*. By using this definition, all data regarding the dependence of the aspect ratio on specific latex characteristics can be rescaled to describe the aspect ratio as a function of *N*, with the concentration of latex particles left constant. The results imply that the aspect ratio arises from a balance of attractive and repulsive forces between the latex surface and the growth surface of the crystal (i.e., the basal plane of zincite) within the interaction volume. Considering these assumptions, an algorithm can be defined that describes the aspect ratio of the resulting crystals over three orders of magnitude in the surface-group density in the corona and size variations of the latex from 60 to 240 nm. We are not aware of a similar and, moreover, quantitative approach in the area of mineralization and/or biomineralization that relates morphological features to variations in chemical structure.

A further conclusion is that the latex has very little, if any, influence on nucleation density. This is deduced from the study of the size distribution of the crystals obtained at different concentrations of the same type of latex. However, the width of the size distribution seems to become narrower at increasing latex concentrations, which may indicate that Ostwald ripening is suppressed in the presence of the latex.

Increasing amounts of the interactive latex particles become incorporated into the growing crystals at increasing overall concentration in the crystallizing system. Hybrid materials that contain up to approximately 10 wt % of latex occluded in the crystals are formed without causing a deterioration in the long-range order in the crystalline material. The polymer can be removed by thermolysis or by dissolution in organic solvents to leave porous crystals of zinc oxide behind. This observation may inspire further developments in the application of zinc oxide in catalysis.

Finally, the results and their analysis reported here demonstrate that morphology control can be very effective without involving topochemically defined interactions between the growth surface and the additive. Poisoning of growth centers, such as dislocations that emerge at the surface and unspecific interactions that control the approach of the additive to the crystal surface, are sufficient to account quantitatively for the dependence of the aspect ratio on the chemical composition of the latex corona. In other words, topochemi-

  

cal and "specific recognition" phenomena are of less importance in this case. The latex particles of chemically structured corona may even be good models to mimic the behavior of globular proteins in biomineralization.

## Experimental Section

Chemicals were supplied by Aldrich (highest purity available) and were used as received, unless otherwise stated. The water used was Milli-Q.

**Synthesis, purification and characterization of latexes**: The latexes listed in Table 1 were prepared in a similar way to that described by Landfester et al.,[38,39] by miniemulsion polymerization with styrene (Fluka, puriss., $\geq$99.5%) and a small amount of one of the second functional comonomers: acrylic acid (**1**), maleic acid (**2**, Janssen Chimica, $\geq$99%), ethylene glycol methacrylate phosphate (**3**), methacrylonitrile (**4**), 2-allylphenol (**5**), vinyl benzyl trimethylammonium chloride (**6**). The monomers (11.52 g of styrene and 0.48 g of comonomer; 12 g of styrene in the case of latex **S0**) were mixed with hexadecane (500 mg) and 2,2′-azobis(2-methylbutyronitrile) (AMBN, Wako Pure Chemical Industries) (240 mg). The aqueous phase was prepared by dissolving Lutensol AT50 (BASF, 3.0 g) in water (48 g). Both the oil and aqueous phases were stirred separately for 30 min and then mixed and stirred for 45 min. The miniemulsion was achieved by ultrasonification for 7 min (Branson Digital Sonifier 250-D; 70% intensity, pulse 1.0 s, pause 0.1 s), followed by cooling in an ice-water bath to avoid polymerization due to heating. The reaction occurred at 72°C under an argon atmosphere and was stopped after 8 h. In the latexes **S2**, **S3**, and **S6**, potassium persulfate (25 mg) was added after 6 h to graft oligomeric, hydrophilic free radicals onto the corona. The resulting latexes were filtered and purified by centrifuging in a disposable Ultrafree-15 centrifugal filter device with a membrane Biomax 50 kDa (Millipore).

The latexes listed in Table 3 and Figure 10 were prepared independently of, but analogously to, those described above. The latex diameters and the surface-charge densities were tuned by selecting the optimal amounts of surfactant and acrylic acid. Various amounts of acrylic acid were mixed with styrene (6 g), hexadecane (250 mg), and AMBN (250 mg). This oil phase was added to the aqueous phase, prepared from various amounts of Lutensol AT50 dissolved in water (24 g). The mixture was stirred as described previously and ultrasonified for 60 s (UD-20 by Techpan, level 5). In this case, the reaction time was 2 h.

The particle size was measured by conducting photon correlation spectroscopy at a fixed angle of 90° with a Malvern Zetasizer 3000HS. Solid contents were determined by drying a portion of emulsion (0.8 g) at 40°C under vacuum for 12 h. The surface-charge density of the latex particles was estimated by polyelectrolyte titration: a pertinent quantity of latex was titrated with a ~0.001 N solution of poly(diallyl dimethylammonium chloride) (poly-DADMAC, Mütek Analytic, $M$ distribution of 40000–100000 g mol$^{-1}$) by using an automatic titration unit Metrohm 702 SM Titrino combined with a particle-charge detector Mütek PCD 03-pH, after adjusting the pH to ~9.5 with a suitable solution of NaOH. The exact concentration of the poly-DADMAC solution was determined by titration with the anionic standard sodium polyethensulphonate (Mütek Analytic, 19100 g mol$^{-1}$, 0.001 N). The surface-charge density was calculated by dividing the number of charged groups $N_{ch}$ by the total surface area of the latex particles $A_{total}$. $N_{ch}$ was obtained by multiplying the number of moles of charged groups (obtained from the titration results) by Avogadro's number $N_A$. The mass of a particle was calculated by assuming a spherical geometry for the latex particles and by approximating the density of the latex to 1 g cm$^{-3}$. By using the mass of a particle and the total mass of the titrated sample, it is possible to calculate the number of latex particles and $A_{total}$.

**Synthesis of ZnO crystals**: A triple-neck flask containing a solution of $Zn(NO_3)_2 \cdot 6H_2O$ (Fluka, $\geq$99%, 0.446 g, 1.50 mmol) in water (95$-x$ mL) was placed in an oil bath and heated at 95°C under reflux and continuous magnetic stirring. The pertinent quantity of latex emulsion ($x$ mL, $x=0$ in the case of the reference sample) was added to the reaction flask. After achieving thermal equilibrium, the reaction was started by adding hexamethylenetetramine (HMTA, 0.210 g, 1.50 mmol) dissolved in water (5 mL). After 90 min, the reaction mixture was cooled in an ice-water bath and the precipitate was separated by centrifugation, washed several times with water, and dried under vacuum at 40°C. To obtain the required quantities, the samples used in the study of the effect of additive concentration (Figures 4–8 and Table 2) were prepared similarly, but by doubling the volume of the solution (total volume after addition of the HMTA solution was 200 mL) and also multiplying by a factor of two the concentration of the reactants ($Zn(NO_3)_2 \cdot 6H_2O$: 1.784 g, 6.00 mmol; HMTA: 0.840 g, 6.00 mmol). In this case, the reaction was performed in a jacketed reactor connected to a thermostated water circulator, which allowed precise control of the temperature. The reaction temperature, reaction time, and product treatment were as previously indicated.

**Powder characterization**: Scanning electron microscopy (SEM) micrographs were recorded by using a field emission microscope LEO EM1530 Gemini. Particle-size histograms and distributions were obtained statistically by measuring the dimensions of at least 100 crystals with the software ImageJ.[56]

X-ray diffractograms (XRD) were registered by using a Seifert XRD 3000 TT diffractometer with $Cu_{K\alpha}$ radiation ($\lambda = 1.54$ Å).

Thermogravimetric analysis (TGA) was conducted by using a balance Mettler TG50 under an oxygen atmosphere and with a heating rate of 10°C min$^{-1}$ from RT→600°C.

## Acknowledgements

We are especially grateful to Dr. Laurent Herschke for his invaluable help with the latex synthesis and for the many scientific discussions. We also thank Dr. Patrice Castignolles and Dr. Britt Minch for the corrections and comments on the manuscript, and Rodrigo Cordeiro for assistance in the mathematical treatment of some data. The Max Planck Society is acknowledged for financial support. R.M.E. also acknowledges financial support from the Deutsche Akademische Austauschdienst (DAAD) and Foundation "la Caixa", as well as from the European Commission (Marie Curie Fellowship, HPMT-CT-2000–00015). BASF is thanked for the supply of Lutensol AT50.

[1] S. Mann, *Biomineralization*, Oxford University Press, New York, **2001**.
[2] *Biomineralization* (Eds.: P. M. Dove, J. J. De Yoreo, S. Weiner), Mineralogical Society of America, Geochemical Society, Washington, **2003**.
[3] *Biomineralization* (Ed.: E. Baeuerlein), Wiley-VCH, Weinheim, **2003**.
[4] a) E. Matijević, *Langmuir* **1994**, *10*, 8–16; b) E. Matijević, *J. Eur. Ceram. Soc.* **1998**, *18*, 1357–1364.
[5] W. Tremel, *Angew. Chem.* **1999**, *111*, 2311–2315; *Angew. Chem. Int. Ed.* **1999**, *38*, 2175–2179.
[6] a) H. Cölfen, *Curr. Opin. Colloid Interface Sci.* **2003**, *8*, 23–31; b) S. H. Yu, H. Cölfen, M. Antonietti, *J. Phys. Chem. B* **2003**, *107*, 7396–7405; c) S. H. Yu, H. Cölfen, K. Tauer, M. Antonietti, *Nat. Mater.* **2005**, *4*, 51–55.
[7] a) M. Faatz, F. Gröhn, G. Wegner, *Adv. Mater.* **2004**, *16*, 996–1000; b) M. Faatz, F. Gröhn, G. Wegner, *Mater. Sci. Eng. C* **2005**, *25*, 153–159.
[8] M. Balz, H. A. Therese, J. X. Li, J. S. Gutmann, M. Kappl, L. Nasdala, W. Hofmeister, H. J. Butt, W. Tremel, *Adv. Funct. Mater.* **2005**, *15*, 683–688.
[9] S. V. Dorozhkin, M. Epple, *Angew. Chem.* **2002**, *114*, 3260–3277; *Angew. Chem. Int. Ed.* **2002**, *41*, 3130–3146.
[10] M. Vallet-Regí, J. M. González-Calbet, *Prog. Solid State Chem.* **2004**, *32*, 1–31.

  

[11] L. M. Qi, H. Cölfen, M. Antonietti, *Chem. Mater.* **2000**, *12*, 2392–2403.
[12] S. Libert, V. Gorshkov, V. Privman, D. Goia, E. Matijević, *Adv. Colloid Interface Sci.* **2003**, *100*, 169–183.
[13] a) L. M. Qi, H. Cölfen, M. Antonietti, *Nano Lett.* **2001**, *1*, 61–65; b) L. M. Qi, H. Cölfen, M. Antonietti, M. Li, J. D. Hopwood, A. J. Ashley, S. Mann, *Chem. Eur. J.* **2001**, *7*, 3526–3532; c) M. Li, H. Cölfen, S. Mann, *J. Mater. Chem.* **2004**, *14*, 2269–2276.
[14] F. Shieh, A. E. Saunders, B. A. Korgel, *J. Phys. Chem. B* **2005**, *109*, 8538–8542.
[15] S. Kar, S. Chaudhuri, *J. Phys. Chem. B* **2005**, *109*, 3298–3302.
[16] X. S. Fang, C. H. Ye, L. D. Zhang, Y. H. Wang, Y. C. Wu, *Adv. Funct. Mater.* **2005**, *15*, 63–68.
[17] a) S. H. Yu, H. Cölfen, M. Antonietti, *Chem. Eur. J.* **2002**, *8*, 2937–2945; b) S. H. Yu, M. Antonietti, H. Cölfen, J. Hartmann, *Nano Lett.* **2003**, *3*, 379–382.
[18] D. Grosso, G. Illia, E. L. Crepaldi, B. Charleux, C. Sanchez, *Adv. Funct. Mater.* **2003**, *13*, 37–42.
[19] A. K. Gupta, M. Gupta, *Biomaterials* **2005**, *26*, 3995–4021.
[20] S. Eiden-Assmann, J. Widoniak, G. Maret, *Chem. Mater.* **2004**, *16*, 6–11.
[21] Z. L. Wang, *J. Phys.: Condens. Matter* **2004**, *16*, R829-R858.
[22] S. J. Pearton, D. P. Norton, K. Ip, Y. W. Heo, T. Steiner, *Prog. Mater. Sci.* **2005**, *50*, 293–340.
[23] D. C. Look, B. Claflin, Y. I. Alivov, S. J. Park, *Phys. Status Solidi A* **2004**, *201*, 2203–2212.
[24] M. Andrés-Vergés, M. Martínez-Gallego, *J. Mater. Sci.* **1992**, *27*, 3756–3762.
[25] a) S. Musić, D. Đragčević, M. Maljković, S. Popović, *Mater. Chem. Phys.* **2002**, *77*, 521–530; b) S. Musić, S. Popović, M. Maljković, D. Đragčević, *J. Alloys Compd.* **2002**, *347*, 324–332.
[26] L. N. Wang, M. Muhammed, *J. Mater. Chem.* **1999**, *9*, 2871–2878.
[27] H. Y. Xu, H. Wang, Y. C. Zhang, W. L. He, M. K. Zhu, B. Wang, H. Yan, *Ceram. Int.* **2004**, *30*, 93–97.
[28] J. E. Rodríguez-Paez, A. C. Caballero, M. Villegas, C. Moure, P. Durán, J. F. Fernández, *J. Eur. Ceram. Soc.* **2001**, *21*, 925–930.
[29] a) A. P. Almeida de Oliveira, J. F. Hochepied, F. Grillon, M. H. Berger, *Chem. Mater.* **2003**, *15*, 3202–3207; b) J. F. Hochepied, A. P. Almeida de Oliveira, *Solid State Phenom.* **2003**, *94*, 171–176.
[30] Z. S. Hu, G. Oskam, P. C. Searson, *J. Colloid Interface Sci.* **2003**, *263*, 454–460.
[31] S. A. Vorobyova, A. I. Lesnikovich, V. V. Mushinskii, *Mater. Lett.* **2004**, *58*, 863–866.
[32] T. Trindade, J. D. Pedrosa de Jesus, P. O'Brien, *J. Mater. Chem.* **1994**, *4*, 1611–1617.
[33] D. R. Chen, X. L. Jiao, G. Cheng, *Solid State Commun.* **1999**, *113*, 363–366.
[34] M. Öner, J. Norwig, W. H. Meyer, G. Wegner, *Chem. Mater.* **1998**, *10*, 460–463.
[35] a) A. Taubert, D. Palms, O. Weiss, M. T. Piccini, D. N. Batchelder, *Chem. Mater.* **2002**, *14*, 2594–2601; b) A. Taubert, G. Glasser, D. Palms, *Langmuir* **2002**, *18*, 4488–4494; c) A. Taubert, C. Kubel, D. C. Martin, *J. Phys. Chem. B* **2003**, *107*, 2660–2666.
[36] G. Wegner, P. Baum, M. Müller, J. Norwig, K. Landfester, *Macromol. Symp.* **2001**, *175*, 349–355.
[37] S. H. Yu, H. Cölfen, *J. Mater. Chem.* **2004**, *14*, 2124–2147.
[38] K. Landfester, N. Bechthold, F. Tiarks, M. Antonietti, *Macromolecules* **1999**, *32*, 5222–5228.
[39] F. Tiarks, K. Landfester, M. Antonietti, *Langmuir* **2001**, *17*, 908–918.
[40] The use of Lutensol AT50 in miniemulsion polymerization and the dependence of particle size on the concentration of surfactant have been studied in the following: a) N. Bechtold, PhD thesis, Universität Potsdam (Germany), **2000**; b) N. Bechthold, F. Tiarks, M. Willert, K. Landfester, M. Antonietti, *Macromol. Symp.* **2000**, *151*, 549–555.
[41] K. Landfester, N. Bechthold, S. Forster, M. Antonietti, *Macromol. Rapid Commun.* **1999**, *20*, 81–84.
[42] S. Kirsch, A. Doerk, E. Bartsch, H. Sillescu, K. Landfester, H. W. Spiess, W. Maechtle, *Macromolecules* **1999**, *32*, 4508–4518.
[43] X. Guo, A. Weiss, M. Ballauff, *Macromolecules* **1999**, *32*, 6043–6046.
[44] G. Fritz, V. Schadler, N. Willenbacher, N. J. Wagner, *Langmuir* **2002**, *18*, 6381–6390.
[45] C. F. Lee, *Polymer* **2002**, *43*, 5763–5769.
[46] H. De Bruyn, R. G. Gilbert, J. W. White, J. C. Schulz, *Polymer* **2003**, *44*, 4411–4420.
[47] P. Borget, F. Lafuma, C. Bonnet-Gonnet, *J. Colloid Interface Sci.* **2005**, *285*, 136–145.
[48] K. H. Wassmer, U. Schroeder, D. Horn, *Makromol. Chem.* **1991**, *192*, 553–565.
[49] K. Böckenhoff, W. R. Fischer, *Fresenius J. Anal. Chem.* **2001**, *371*, 670–674.
[50] R. H. Müller, *Zetapotential und Partikelladung in der Laborpraxis*, Wissenschaftliche Verlagsgesellschaft, Stuttgart, **1996**.
[51] R. H. Müller, S. Raimund, *Teilchengrößenmessung in der Laborpraxis*, Wissenschaftliche Verlagsgesellschaft, Stuttgart, **1996**.
[52] P. Ponasewicz, R. Littbarski in *Current Topics in Materials Science, Vol. 7* (Ed.: E. Kaldis), North-Holland Publishing, Amsterdam, **1981**, pp. 387–394.
[53] H. P. Klug, L. E. Alexander, *X-Ray Diffraction Procedures for Polycrystalline and Amorphous Materials*, John Wiley, New York, **1974**.
[54] The contribution of the Kβ to the peak form was taken into account by fitting the peaks to double Lorentzian curves.
[55] J. Israelachvili, *Intermolecular and Surface Forces*, Academic Press, London, **2002**.
[56] Public domain program to be found under http://rsb.info.nih.gov/ij, National Institute of Health (NIH).

Received: July 21, 2005
Published online: October 14, 2005

  